Concept Paper

Not peer-reviewed version

Price Based Load Frequency Control With Bidirectional Charging Mechanism With EV

Yogeshkumar Prajapati *

Posted Date: 15 February 2023

doi: 10.20944/preprints202302.0254.v1

Keywords: AGC; Electrical Vehicle; ABT; Fuzzy Logic

Concept Paper

Price Based Load Frequency Control with Bidirectional Charging Mechanism with EV

Dr. Y R Prajapati

BVM Engineering College, Electrical Engineering Department, Vallabh Vidyanagar;
yrprajapati@bvmengineering.ac.in

Abstract: Contract violations, uncontracted load, and the alternating nature of electricity are the key causes of the frequency irregularity and Unscheduled Interchange (UI) / Deviation Settlement pricing in a restructured organized smart grid. These variations cause the frequency to fluctuate. The topic of frequency variation is discussed in this paper under various market circumstances. To correct frequency discrepancies under various market conditions, a fleet of electrical vehicles (EV) is offered as a distributed energy storage (DES). A bidirectional charger with a PI controller is suggested for the EV bidirectional power transfer. It is suggested to use a fuzzy logic (FL) controller to modify the proportional-integral (PI) controller gains. It has been noted that utilizing such a new approach lowers the UI prices.

Keywords: AGC; Electrical Vehicle; ABT; Fuzzy Logic

1. Introduction

As a fast-responding device against frequency variations, a grid-connected fleet of EVs is a superior alternative [1]. PI controllers are typically used to track the load continually when charging and discharging the EV battery [2]. However, due to nonlinearity load uncertainty, the PI controller's performance suffers [3]. As a result, a fuzzy PI controller is appropriate. It can track more accurately than the PI controller, resulting in lower frequency deviations and shorter settle down times [4]. This article examined how to use the FG controller [18] to modify the PI controller gain. It is suggested to use a power system with a thermal-hydro and thermal non-reheat system for AGC functioning. The DISCOM Participation Matrix DPM was used to make contracts between DISCOs and GENCOs in the restructured environment [5]. Load oscillation is used to learn frequency aberrations in the power system. The Poolco-based market and the Bilateral market are investigated for the study. The load violation conditions were performed and simulated. Finally, due to the battery's frequent response counter to load variation, a fleet of electric and hybrid vehicles (EVs) with larger battery energy storage [15], as well as accessory service [16], has been proposed. This work presents a real-time [17] [19] V2G and G2V control application.

2. Description of the Model

A grid-connected distributed energy storage system employing an EV has been proposed in two regions, as shown in Figure 1. Under Poolco-based and bilateral contracts, the DPM is utilized by AGC [6]. The frequency fluctuations are made worse by the RESs and the load's unpredictability. The EV model is suggested. Simulated is the bidirectional charging controller operation followed by the frequency characteristic. For the simulation, the PI controller and FGPI controllers are used.

3. Mathematical Modelling of Two Areas of Restructured Power System

To understand the two-area relationship, the DISCOM Participation Matrix (DPM) is shown in Table I [6]. In Area 1, GENCO-DISCO pairs 11, 12, 21, 22, 31, 32, 41, and 42 are taken into consideration. Likewise, the numbers 13, 14, 23, 24, 33, 34, 43, and 44 are used in Area 2 to symbolize these pairs. It reflects a contract between GENCO and DISCO, who are both represented by Eq (1).

Preprints (www.preprints.org) | NOT PEER-REVIEWED | Posted: 15 February 2023 doi:10.20944/preprints202302.0254.v1

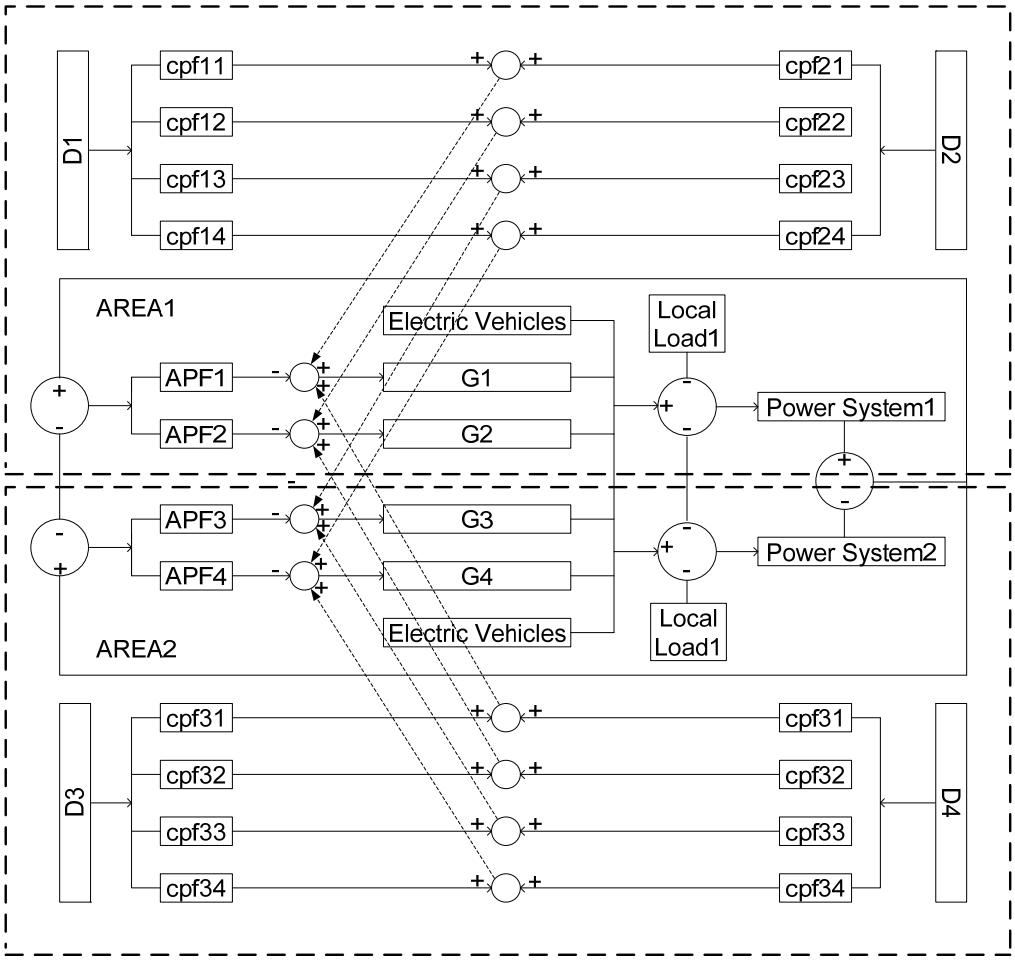

Figure 1. Two areas restructured power system.

Table 1. DPM Matrix.

		A1		A2	
		D1	D2	D3	D4
A1	G1	11	12	13	14
	G2	21	21	23	24
A2	G3	31	32	33	34
	G4	41	42	43	44

A= Area, G=GENCO, D=DISCO.

$$DPM = \begin{bmatrix} cpf_{11} & cpf_{12} & cpf_{13} & cpf_{14} \\ cpf_{21} & cpf_{22} & cpf_{23} & cpf_{24} \\ cpf_{31} & cpf_{32} & cpf_{33} & cpf_{34} \\ cpf_{41} & cpf_{42} & cpf_{43} & cpf_{44} \end{bmatrix} \quad (1)$$

The contract participation factor (cpf) indicates that the agreement data is transmitted. It is advantageous to use tail electricity by using load from GECNO and DISCO. The cpf may be determined from Eq (2). The diagonal parts provide details about the cooperation between the regional GENCOs and DISCOs. Details regarding a contract between the DISCOs in one region and the GENCOs in another area are provided by the off-diagonal components. Consider a scenario where DISCO3 must acquire 150 MW of power, of which 30 MW must come from DISCO1, 45 MW

Preprints (www.preprints.org) | NOT PEER-REVIEWED | Posted: 15 February 2023 doi:10.20944/preprints202302.0254.v1

from DISCO2, 60 MW from DISCO3, and 15 MW from DISCO4. Eq. (1) establishes the DPM's parameters (2). Eq. allows for the calculation of the fluctuations in GENCO power (3).

T

$$\sum_i cpf_{ij} = 1 \tag{2}$$

$$cpf_{13} = \frac{30}{150} = 0.2, \quad cpf_{23} = \frac{45}{150} = 0.3,$$
$$cpf_{33} = \frac{60}{150} = 0.4, \quad cpf_{43} = \frac{15}{150} = 0.1.$$

The deed of power to supply by ith GENCO is given by,

$$\Delta P_{gi} = \sum_{j=1}^{DISCO4} cpf_{ij} \Delta P_{Lj} \tag{3}$$

Where ΔP_{Lj} represents DISCOj total load demand as presented in Eq. (4).

$$\Delta P_{L1,LOC} = \Delta P_1 + \Delta P_2, \quad \Delta P_{L2,LOC} = \Delta P_{31} + \Delta P_4 \tag{4}$$

The tie line scheduled power is determined by Equations (5) and (6) due to variations in the load (6).

$$\Delta P_{tie1-2,scheduled} = (denad\ of\ DISCOs\ in\ area\ II\ from\ GENCOs\ in\ area\ 1) - (denand\ of\ DISCOs\ in\ area\ I\ from\ GENCOs\ in\ area\ II) \tag{5}$$

$$\Delta P_{tie12,schedule} = \sum_{i=1}^{2}\sum_{j=3}^{4} cpf_{ij} \Delta P_{Lj} - \sum_{j=3}^{4}\sum_{i=1}^{2} cpf_{ij} \Delta P_{Lj} \tag{6}$$

The tie line power error is given by Eq. (7).

$$\Delta P_{tie1-2,actual} = \left(\frac{2\pi T_{12}}{s}\right)(\Delta F_1 - \Delta F_2) \tag{7}$$

$$\Delta P_{tie1-2,error} = \Delta P_{tie1-2,actual} - \Delta P_{tie1-2,scheduled} \tag{8}$$

The tie line power error Eq. (8) supports to cause of Area Control Error (ACE) in the corresponding area [6]. This ACE can be calculated by Eq. (9).

$$ACE_1 = B_1 \Delta f_1 + \Delta P_{tie1-2,error}, \quad ACE_2 = B_2 \Delta f_2 + a_{12} \Delta P_{tie1-2,error} \tag{9}$$

$$a_{12} = -\frac{P_{r1}}{P_{r2}} \tag{10}$$

Where, P_{r1} = Area 1 rating, MWs

P_{r2} = Area 2 rating, MWs.

By providing power to the associated DISCO, the DPM aids GENCO. The input has applied the abrupt load fluctuation. Due to the imbalance between the load and supply, the signal of Load Frequency Control (LFC) is now generated by the ACE. The ACE participation matrix measures the

Preprints (www.preprints.org) | NOT PEER-REVIEWED | Posted: 15 February 2023 doi:10.20944/preprints202302.0254.v1

LFC signal forwarding as, and. In an ACE generation that is distributed to the GENCOs in accordance with apfs, the controller performs a crucial job. The integral control law is used to adjust the controller gain (11).

$$U_i = -K_{1i} \int ACE_i dt \tag{11}$$

Figure 2 depicts the N-area IPS's mathematical representation. The model has now been updated to incorporate an EV battery discharge dynamic model, a wind turbine model, and a thermal plant with a non-reheat unit. The Area Participation Factor (APF) is used by the System Operator (SO) to distribute the ACE signal to GENCOs and the LFC signal to the aggregators from the Control Centre. The aggregators transmit the LFC signal to each and every EV. Thanks to the bidirectional charger, the EV may supply electricity to the grid.

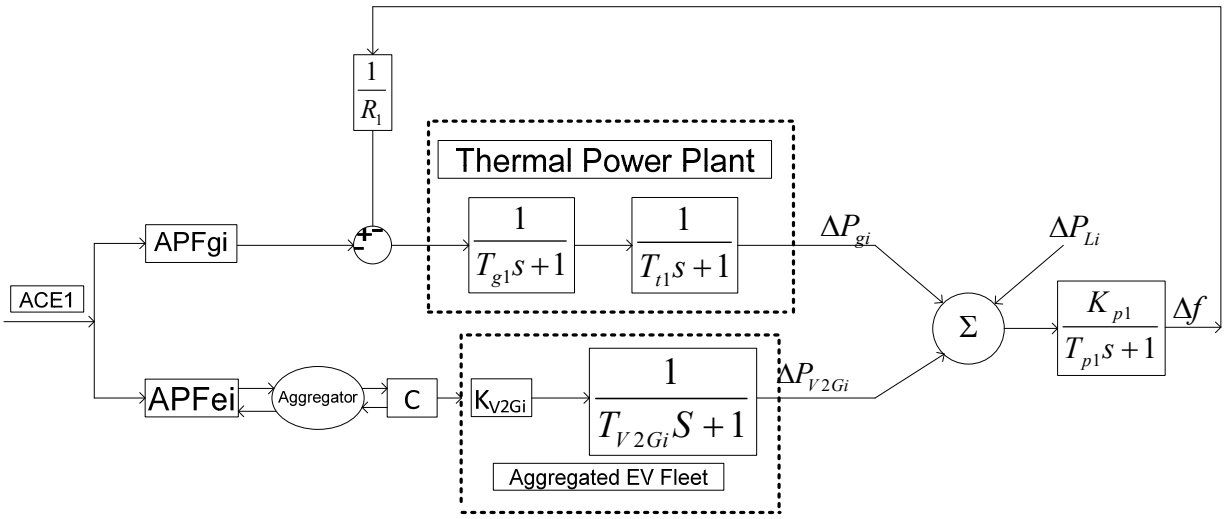

Figure 2. The grid frequency regulation proposed scheme. (C=Controller).

4. EV Battery Charging Controller

To achieve optimal performance, PI controllers can monitor changes. When operating circumstances change, a PI controller, however, is unable to achieve the expected outcomes [7]. Frequency variations are caused by intrinsic intricacy, nonlinearity, or load improbability in the power system [8]. Due to the flexible and straightforward functioning of fuzzy logic, PI controller gains have been tweaked [9] because PI controllers are unable to provide the appropriate result. Figure 3 depicts the FGPI controller's logic.

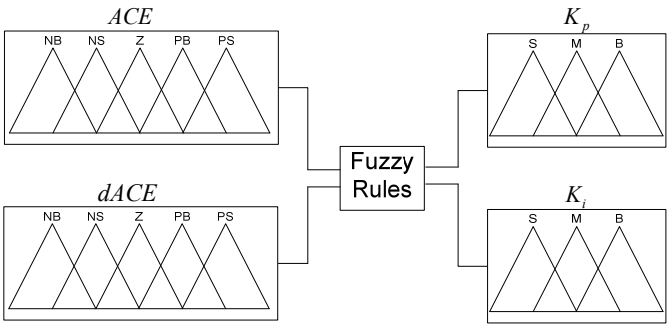

Figure 3. A fuzzy-based tuned PI controller's block diagram.

Table 7.1 shows the fuzzy control FG rules and MF. The MF "Triangular" is employed. Here, two numbers of input and two numbers of output are available. An ACE and dACE are inputs, and the K_P and K_I are outputs of the PI controller. As indicated in Table 2, there are 25 fuzzy rules defined to map the inputs as ACE and ACE.

Preprints (www.preprints.org) | NOT PEER-REVIEWED | Posted: 15 February 2023 doi:10.20944/preprints202302.0254.v1

Rule: The output is S if the first input, ACE, is NB and ACE is NB.

The fuzzy logic rules for fine-tuning KP and KI are shown in Table 2. For secondary frequency regulation, the typical controller is employed. The PI controller is often applied in practice based on preset parameters. This controller can provide optimal performance while continuously following the load. In the face of alterations in the operational environment, the PI is unable to deliver the anticipated outcomes [10].

Table 2 shows the fuzzy logic rules used to tune K_P and K_I. The typical controller is utilized for secondary frequency control. In practice, the PI controller is typically employed based on pre-specified values. This controller can constantly monitor the load and provide optimal performance. The PI cannot produce expected results when operational conditions vary [10]. As illustrated in Fig 2, an intelligent fuzzy logic is ideal for tweaking PI controller gains such as K_P and K_I [11-12].

Table 2. Fuzzy logic Rules.

Input1 →		ACE				
Input2		NB	NS	Z	PS	PB
↓	NB	S	S	M	M	B
	NS	S	M	M	B	VB
ΔACE	Z	M	B	B	VB	VB
	PS	B	B	VB	VB	VB
	PB	B	VB	VB	VVB	VVB

5. Energy Storage

Linear frequency characteristics from 49.7 to 50.04 Hz are studied, as illustrated in Figure 4 [7],[19]. The magnitude of a gradient is proportional to the number of ACEs dispatched. When there is a positive ACE, the LFC signal becomes negative, indicating that the battery charging power for EVs will be increased; when there is a negative ACE, the LFC signal provided to EVs becomes positive, indicating an increase in discharging power [21] [22].

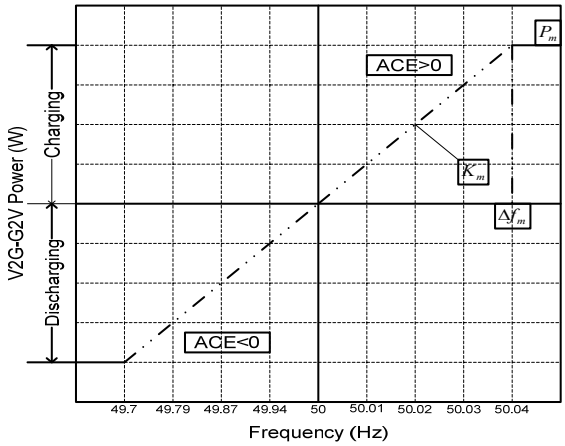

Figure 4. EV battery characteristics.

6. Price-Based Operation

The primary and subsidiary control loops in Figure 6 are depictions of the block diagram in Figure 5. The subsidiary control loop is illustrated here by the Availability Based Tariff (ABT) loop. The ABT consists of three components: variable fee, fixed charge, and unscheduled interchange (UI) charge [13]. Generators respond to frequency alterations in the FGMO's Primary frequency control loop. The UI pricing signal is being used in the secondary frequency control loop [14]. Figure 7 depicts

Preprints (www.preprints.org) | NOT PEER-REVIEWED | Posted: 15 February 2023 doi:10.20944/preprints202302.0254.v1

the statistics of UI charges versus frequency dips for the scenario. The Deviation Settlement Method (DSM) replaces the UI mechanism [20].

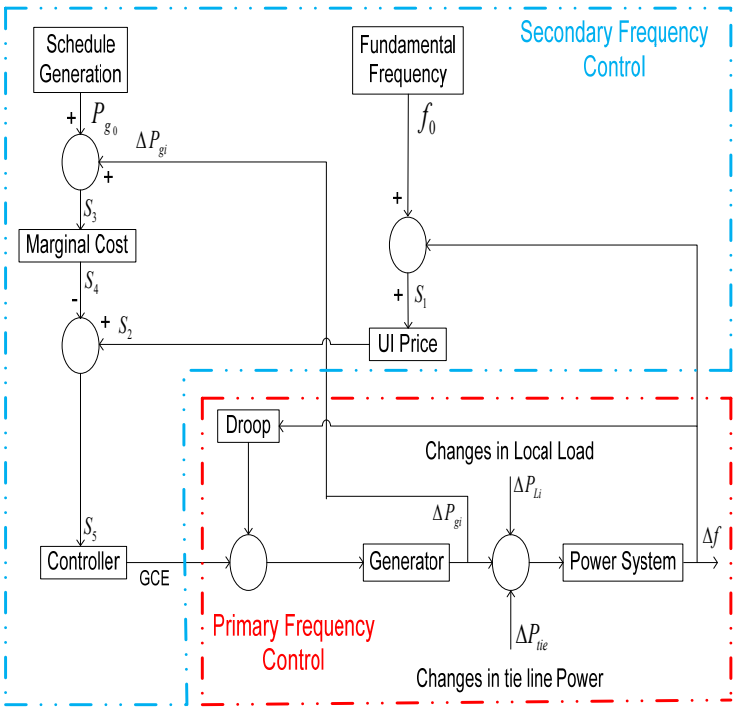

Figure 5. ABT-based AGC loop.

The signal S1 in Figure 6 represents the change in frequency, which is represented by this price-based AGC scheme. Corresponding to CERC, signal S2 denotes the frequency of the UI pricing signal (2016). Signal S3 denotes the accumulation of the planned generation as well as modifications to the generator output. Signal S4 depicts the determined marginal cost. Signal S5, which is the difference between the marginal cost and UI price signals, is used to describe generation control error (GCE). In this instance, generators who earn by raising the generation level have a positive GEC value, while those who profit by lowering the generation level have a negative GEC value. The price-based AGC mathematical modelling is shown in the part that follows.

7. Mathematical Modeling of Price-Based AGC

When the load in the power system steps up or down, the frequency varies by Δf Hz. The fundamental frequency f_0 is multiplied by the frequency variations (Δf) to produce signal S1, Eq (12). The frequency standards released by the relevant year are used to calculate the signal S2 in accordance with the UI charges. Now, S2 is computed using the logic in the flowchart (Figure 6) as described below to produce the GEC S5 Rs/MWh.

During the step variations in the load that the power system experiences, the frequency varies by Hz. In order to produce signal S1 (12), the frequency deviation is added up to the fundamental frequency f_0. Based on the frequency standards released by the relevant year, signal S2 is calculated according to the UI costs. Now, in order to produce the GEC S5 Rs/MWh, S2 is computed in accordance with the subsequent reasoning as indicated in the flow chart (Figure 6).

$$S_1 = \Delta f + f_0 , \tag{12}$$

Where f_0 is the fundamental frequency in Hz

If S_1<=49.7 Hz ; S_2=8032 Rs/MWH

elseif S_1<=50 Hz ; S_2=1780+20856*(50- S_1) Rs/MWH

Preprints (www.preprints.org) | NOT PEER-REVIEWED | Posted: 15 February 2023 doi:10.20944/preprints202302.0254.v1

elseif S_2<=50.05 Hz ; S_2=35600*(50.05- S_1) Rs/MWH

else S_2=0 Rs/MWH.

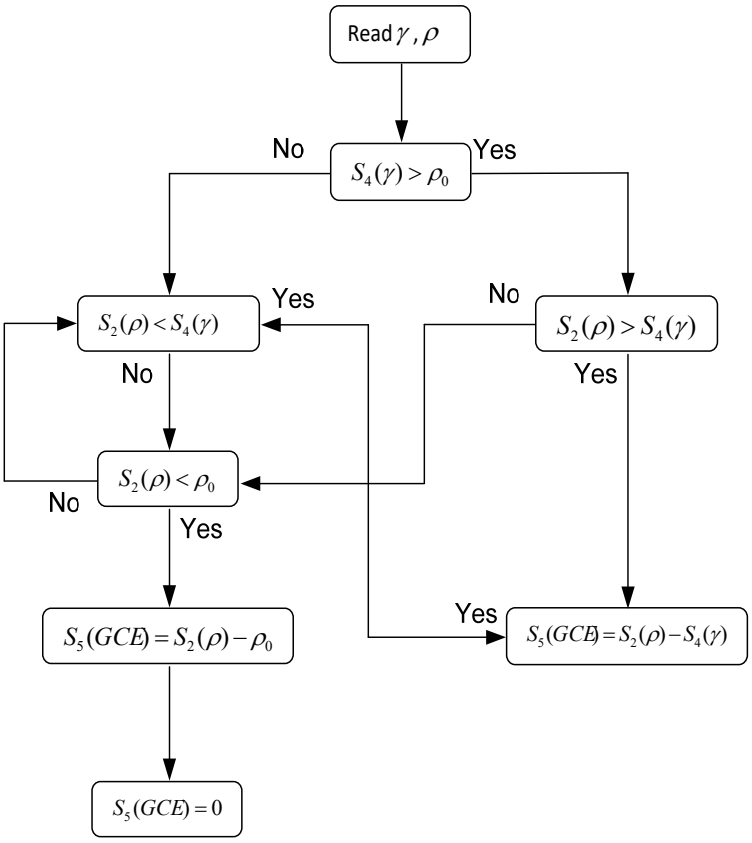

Figure 6. Proposed Flow Chart for GCE Calculation.

S_3 is the difference between the scheduled generation (P_{g0}) MW and the changes in the generator power (ΔP_{gi}) MW as given by Eq. (13).

S3 represents the difference between the scheduled generation (P_{g0}) MW and the variations in generator power
(ΔP_{gi}) MW as calculated by Eq (13).

$$S_3 = P_{g0} + \Delta P_{gi} \tag{13}$$

Now, the signals UI and S_4 (the generator's incremental cost signal) are compared in the signal UI. GEC signal S_5 Eq is generated by the controller. (14). The signal S4 is then output for each generator.

$$S_4 = 2 * c_i * S_3 + b_i \quad \text{Rs/MWh} \tag{14}$$

The positive value of GEC reflects generators who benefit by increasing the generation level, while the negative value of GEC shows generators who profit by decreasing the generation level.

Preprints (www.preprints.org) | NOT PEER-REVIEWED | Posted: 15 February 2023 doi:10.20944/preprints202302.0254.v1

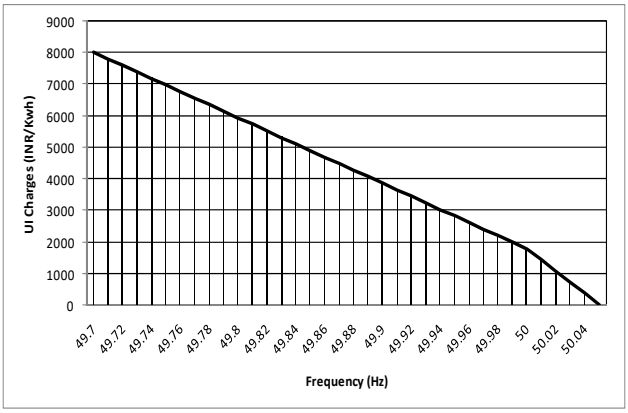

Figure 7. UI price vs frequency graph (CERC, 2016).

8. Results and Discussion:

8.1. Intelligent Price-Based AGC Operation under the Bilateral Transaction

In order to replicate the operation of AGC under the Bilateral Contracts, two isolated area power systems with a combined capacity of 2000 MW and a base MVA of 2000 MVA are used. The Appendix contains the parameters of the isolated network.

8.3. Bilateral Market

A surplus of power on the demand side could lead to contract violations. The local area's generator must provide power because it is an unlicensed source. Here, it is assumed that a load deviation that is not specified in the contract demand—10% surplus power—was increased. the DPM is therefore unchanged. The DPM is presented as an Eq for the bilateral transaction (16). The apf1 = 0.5, apf2 = 0.5, apf3 = 0.5, and apf4 = 0.5 are taken into consideration here.

$$DPM = \begin{bmatrix} 0.5 & 0.25 & 0 & 0.3 \\ 0.2 & 0.25 & 0 & 0 \\ 0 & 0.25 & 1 & 0.7 \\ 0.3 & 0.25 & 0 & 0 \end{bmatrix} \quad (16)$$

It is presumable that both sectors will experience a load variance of 200 MW. Figure 8 (a) to (c) compares the dynamic behaviour under unexpected load changes between the PI controller and the Fuzzy PI Controller (FPC) of an EV bidirectional charger (i). The GENCO variations are displayed in Figure 8 (a) through (d). The more abrupt rise and decline in the frequency of area1 than in area2 were shown in Figure 8 (e) and (f). Figure 8 (g) shows the variations in the UI pricing (Rs/Mwh) (h). Figure 8 shows the tie-line flow (i). The power calculation is presented in Table 4.

Table 4. Power Calculation at GENCOs and Tie Line (Bilateral Transaction).

Deviations in Generation					**Tie**
Unit	G1	G2	G3	G4	**Line**
MW	105	45	195	55	-50

Preprints (www.preprints.org) | NOT PEER-REVIEWED | Posted: 15 February 2023 doi:10.20944/preprints202302.0254.v1

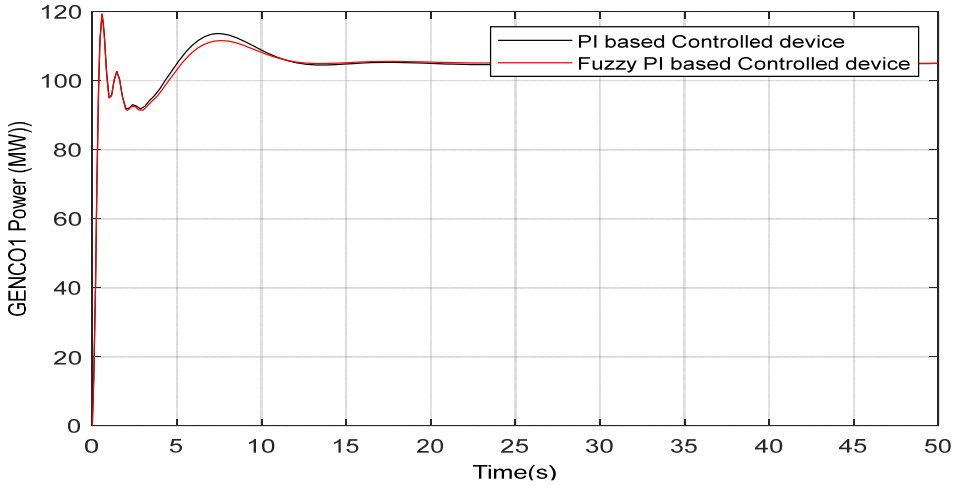

FIGURE 8 (a) Comparison of PI and Fuzzy PI controller outcomes in a bilateral transaction for GENCO1 Power Deviations of Area1

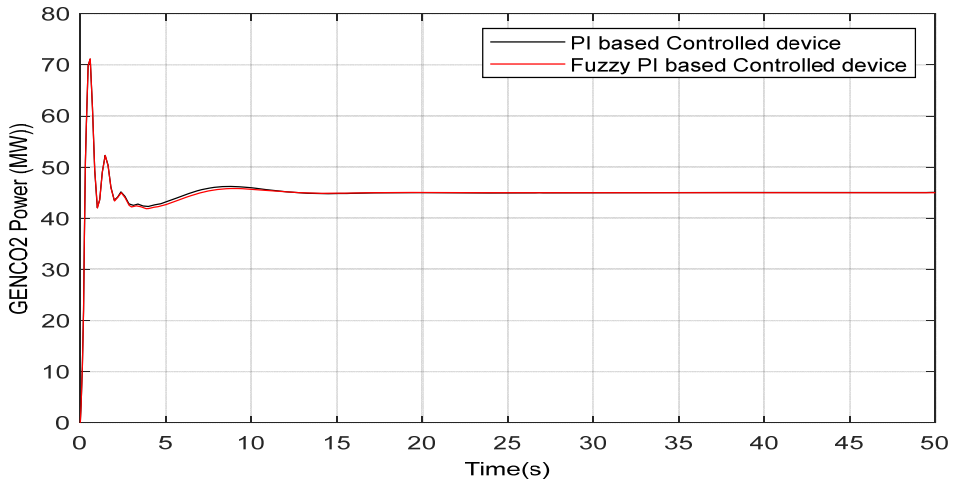

FIGURE 8 (b) Results of a PI and a Fuzzy PI controller in a bilateral transaction for GENCO2 Power Deviations of Area1

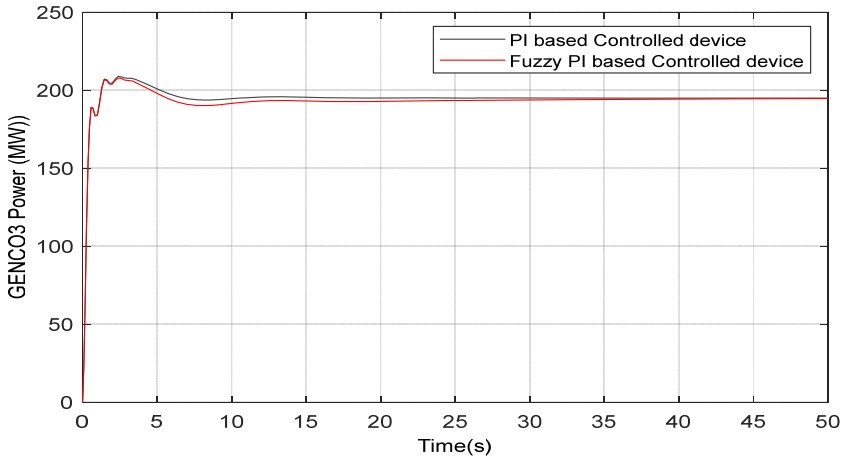

(c)

FIGURE 8 (c) Results of PI and Fuzzy PI controllers in a bilateral transaction for GENCO3 Power Deviations in Area 2.

Preprints (www.preprints.org) | NOT PEER-REVIEWED | Posted: 15 February 2023 doi:10.20944/preprints202302.0254.v1

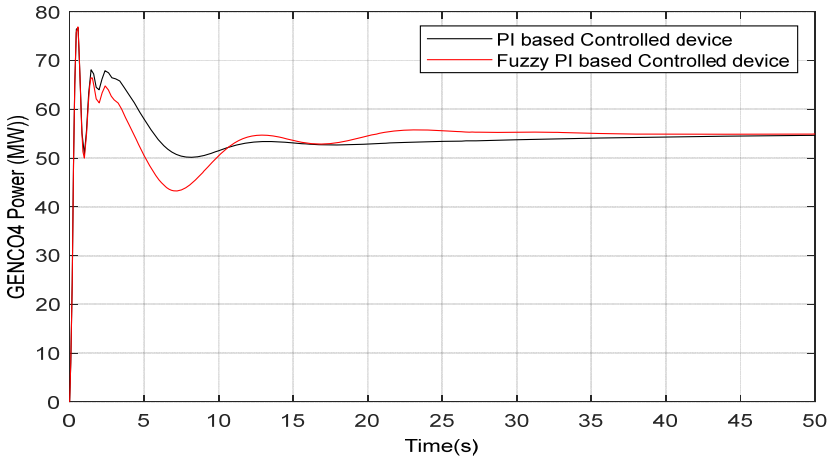

FIGURE 8 (d) Comparison of PI and Fuzzy PI controller results in a bilateral transaction for GENCO4 Power Deviations of Area2.

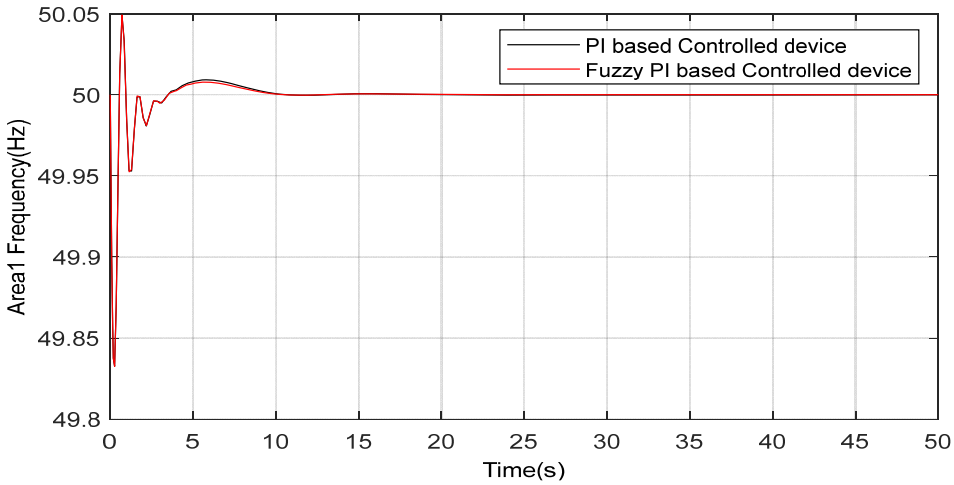

FIGURE 8 (e) Results of a PI and a Fuzzy PI controller in a bilateral transaction for Frequency Deviations of Area1

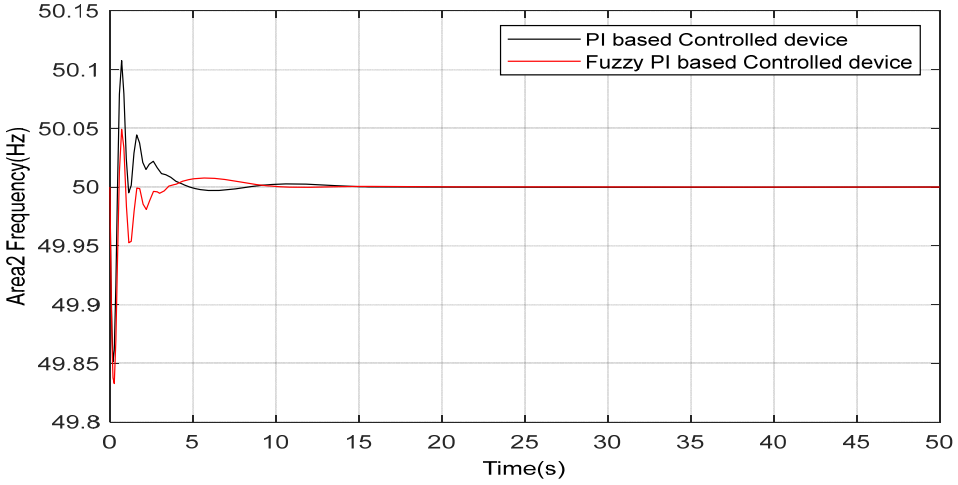

(f)

Preprints (www.preprints.org) | NOT PEER-REVIEWED | Posted: 15 February 2023 doi:10.20944/preprints202302.0254.v1

FIGURE 8 Results of a PI and a Fuzzy PI controller in a bilateral transaction for Frequency Deviations of Area2.

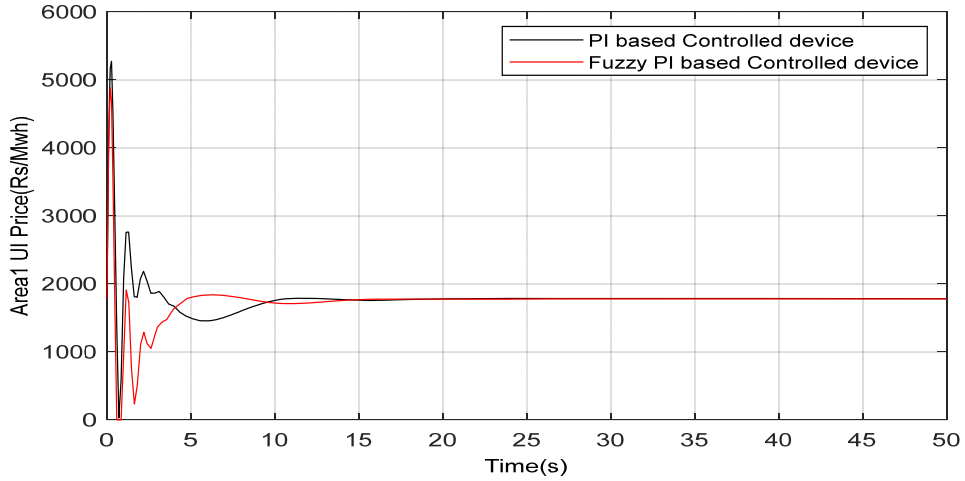

FIGURE 8 (g) Results of a PI and a Fuzzy PI controller in a bilateral transaction for UI Price Deviations of Area1

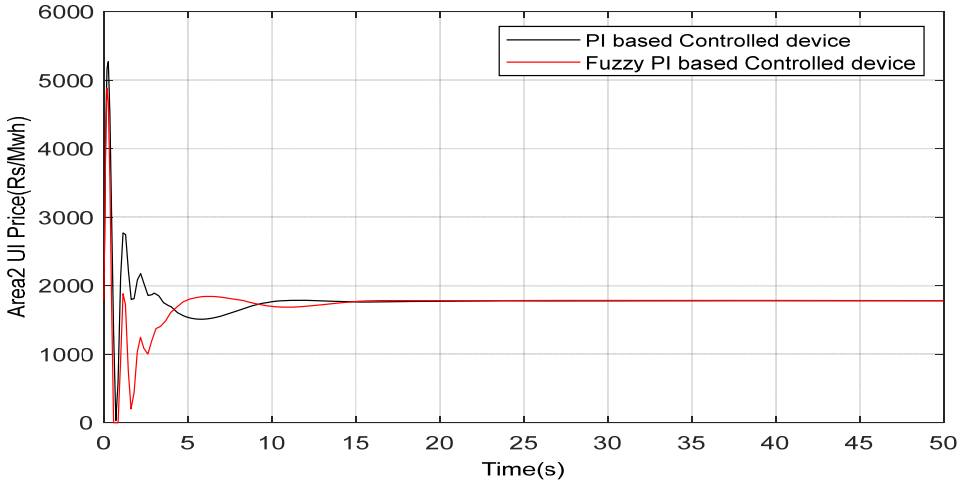

FIGURE 8 (h) Results of a PI and a Fuzzy PI controller in a bilateral transaction for UI Price Deviations of Area2

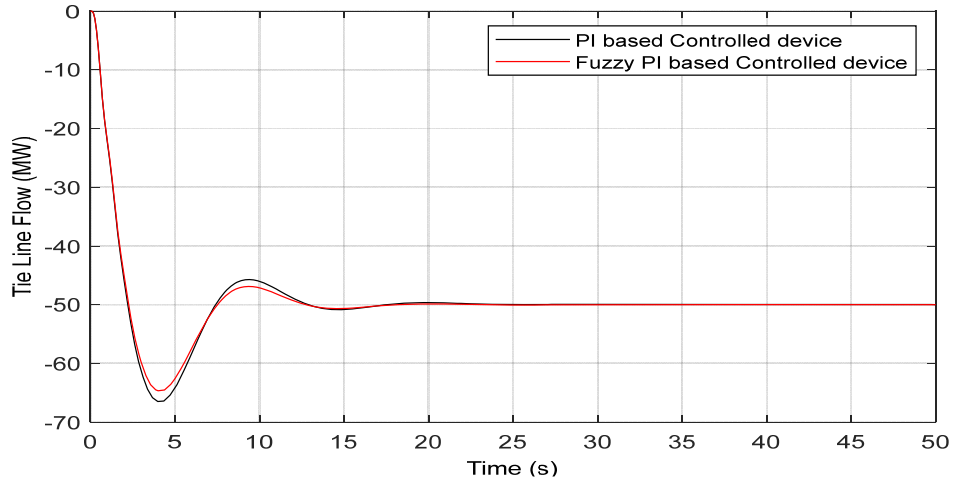

Preprints (www.preprints.org) | NOT PEER-REVIEWED | Posted: 15 February 2023 doi:10.20944/preprints202302.0254.v1

(i)

FIGURE 9 (i) Comparison of PI and Fuzzy PI controllers in a Bilateral Transaction for Tie-Line Flow.

Table 5. Comparison of PI and FGPI Integration.

Device	Settle down Time (s)				Highest Overreaches								Number of Fluctuations			
					>50 Hz				<50 Hz							
	AR1		AR2		AR1		AR2		AR1		AR2		AR1		AR2	
	Fr.	UI	Fr.	UI	Fr.	UI	Fr.	UI	Fr.	UI	Fr.	UI	Fr.	UI	Fr.	UI
PI	13	13	14	14	50.06	0	50.11	0	49.83	5300	49.84	5300	6	6	5	5
FGPI	10	10	10	10	50.05	0	50.05	0	49.83	5300	49.86	5000	5	5	4	4

(Fr.- Frequency, UI- Unscheduled Interchange Charge).

8.6. Bilateral Market

The Area1 frequency operating range for the Proportional Integral (PI) based control device intended for the grid operating in a bilateral market is 50.06 - 49.83 Hz (Figure 8(e)), the UI price trading range is 0 - 5300 Rs/Mwh (Figure 8(g)), the number of oscillations is 13 (Figure 8(e)), and the frequency settle down time is 6 s (Figure 8(e)). Using the Fuzzy rule-based PI controller, the frequency operating range is reduced to 50.04 - 49.86 Hz (Figure 8(e)), the UI price operating range is reduced from 0 to 5000 Rs/Mwh (Figure 8(g)), the number of frequency oscillations is reduced to 10, and the frequency settle down time is reduced to 5 s (Figure 8(e)). In Area 2 with PI controller, the frequency operating range is 50.007 - 49.96 Hz (Figure 8(f)), the UI price operating range is 0 - 2600 Rs/Mwh (Figure 8(h)), there are 7 oscillations, and the frequency settle down period is 11 s (Figure 8(f)). The frequency operating range is reduced to 50.001 - 49.98 Hz (Figure 8(f)), the UI price is reduced to 0 - 2200 Rs/Mwh Figure 8(h)), the frequency settle-down time is reduced to 10 (Figure 8(f)), and the frequency settle down time is reduced to 6 s (Figure 8(f)). When the simulation and Table 5 data were compared, EV gave superior results in terms of a decrease in the operational frequency range, operating range of UI charges, frequency settlement time, and frequency oscillation.

9. Conclusions

The DISCOs and GENCOs of various control zones have a bidirectional contract in the restructured electricity system. The nature of RES in the current IPS is intermittent. It causes power fluctuations that amplify the load-related aberrations. Frequency becomes unstable as a result of the load variations. According to research into many literary genres, storage is necessary for the power system's frequency stability. To reduce frequency fluctuation, a bidirectional charging control system for EVs is proposed. Grid-connected RES is also taken into account. The operator may control the charging process by monitoring the battery SOC level by broadcasting the LFC signal to all EVs. Electric vehicles (EVs) help normalize irregularities in frequency, generator power, tie-line traffic, and UI pricing. An enormous benefit of an EV is that it can function as both a source and a load. PI controllers are used to operating bidirectional chargers. The system modifications may be monitored by the PI controllers. However, PI controllers are unable to provide optimal performance under the diverse working circumstances of the grid. Additional work has been done to fine-tune PI settings using fuzzy logic, and compare findings between the FGPI controller and PI have been achieved. Finally, it can be said that the FGPI controller can deliver better outcomes than the PI controller.

References

[1] Wajahat Khan, Furkan Ahmad and Mohammad Saad Alam," Fast EV charging station integration with grid ensuring optimal and quality power exchange", Engineering Science and Technology, vol.22, pp.143-152,2019.

[2] Hui Cai, Qiyu Chen, Zhijian Guan & Junhui Huang, "Day-ahead optimal charging/discharging scheduling for electric vehicles in microgrids", Protection and Control of Modern Power Systems vol.3(9), pp. 1-15, 2018.

[3] Ronald S. Rebeiro; M. Nasir Uddin," FLC based tuned PI controller for wide speed range operation of IPMSM drive", IEEE PES General Meeting, ISBN: 978-1-4244-6551-4, 25-29 July 2010.

[4] Y R Prajapati and V. N Kamat, "Secondary frequency regulation / Automatic Generation Control under Deregulated Power System along with renewable energy sources using Electric Vehicle / Distributed Energy Storage Systems", IEEE ICEEOT Conf., pp. 34-41, 2016.

[5] Y R Prajapati, V. N Kamat and J J Patel, " Load Frequency Control Under Restructured Power System Using Electrical Vehicle as Distributed Energy Source", J Inst. Eng. India.Ser.B, July 2020.

[6] Vaibhav Donde, "Simulation And Optimization In An AGC System After Deregulation", IEEE Transactions On Power Systems, vol.16, no.3, August 2001.

[7] Diambomba Hyacinthe Tungadio and Yanxia Sun, "Load frequency controllers considering renewable energy integration in power system", Energy Reports, vol.5, pp. 436–453, 2019.

[8] Leonardo Rydin Gorjão, MehrnazAnvari, Holger Kantz, Christian Beck, Dirk Witthaut, Marc Timmeand Benjamin Schäfer," Data-Driven Model of the Power-Grid Frequency Dynamics", IEEE Access, vol.8, pp. 43082-43097, 2020.

[9] Murali, V., Sudha, K.R. Price-based fuzzy automatic generation control for Indian tariff system. Energy System, vol.10, pp. 231–246, 2019. https://doi.org/10.1007/s12667-018-0273-0

[10] D. J. Lee and L. Wang, "Small-signal stability analysis of an autonomous hybrid renewable energy power generation/energy storage system part I: Time-domain simulations," IEEE Trans. Energy Conversion., vol. 23, no. 1, pp. 311-320, 2008.

[11] A. Demiroren, "Automatic Generation Control Using Ann Technique for Multi-Area Power System with SMES Units", Electric Power Components And Systems, vol.32, pp.193-213, Doi: 10.1080/15325000490195989, Jun 2010.

[12] A. Khodabakhshian , R. Hooshmand, "A New PID Controller Design For Automatic Generation Control Of Hydro Power Systems", Electrical Power And Energy Systems vol.32, pp.375–382, 2010.

[13] Naimul Hasan, Ibraheem&Samiuddin Ahmad (2016) ABT Based Load Frequency Control of Interconnected Power System, Electric Power Components and Systems, vol.44(8), pp. 853-863, DOI: 10.1080/15325008.2016.1138160.

[14] AvaniPujara,JigarPujara,GeetaVelhal, Dr S.M. Bakre, Dr V. Muralidhara, Load Frequency Control Under Availability Based Tariff Environment Using Client-Server Communication: A Case Study", International journal of scientific & technology research vol. 8(10), October 2019.

[15] Sandeep Dhundhara, Yajvender Pal Verma, "Capacitive energy storage with optimized controller for frequency regulation in realistic multisource deregulated power system" Energy, Doi: 10.1016/j.energy.2018.01.076; Vol.147, pp.1108-1128, 2018.

[16] Anuj Banshwar, Naveen Kumar Sharma, Yog Raj Sood, Rajnish Shrivastava,"An international experience of technical and economic aspects of ancillary services in deregulated power industry: Lessons for emerging BRIC electricity markets", Renewable and Sustainable Energy Reviews, Doi: 10.1016/j.rser.2018.03.085; Vol.90, ,pp. 774-801 , 2018.

[17] H. Liu, K. Huang, Y. Yang, H. Wei & S. Ma, "Real-time vehicle-to-grid control for frequency regulation with high frequency regulating signal", Protection and Control of Modern Power Systems, Vol.3(13), pp.1-8, 2018.

[18] Shahid Hussain, Mohamed A. Ahmed , Young-Chon Kim ,"Efficient Power Management Algorithm Based on Fuzzy Logic Inference for Electric Vehicles Parking Lot," IEEE Access, DOI: 10.1109/ACCESS.2019.2917297, vol.7, pp. 65467 – 65485, 2019.

[19] VenkateswaranLakshminarayanan , Venkata Gowtam S. Chemudupati, Kaushik Rajashekara , " Real-Time Optimal Energy Management Controller for Electric Vehicle Integration in Workplace Microgrid", IEEE Transactions on Transportation Electrification, Vol.5 (1), pp.175-185, 2019.

[20] Central Electricity Regulatory Commission, India Report 2016, http://www.cercind.gov.in/2017/annual_report/ANE.pdf.

[21] K.M.S.Y. Konara, Mohan Kolhe and Arvind Sharma, "Power flow management controller within a grid connected photovoltaic based active generator as a finite state machine using hierarchical approach with droop characteristics", Renewable Enrgy, vol.155, pp.1021-1031, 2020.

[22] K.M.S.Y. Konara , M.L. Kolhe and Arvind Sharma," Power dispatching techniques as a finite state machine for a standalone photovoltaic system with a hybrid energy storage", AIMS Energy, vol.8(2), pp.214-230, March 2020.

Preprints (www.preprints.org) | NOT PEER-REVIEWED | Posted: 15 February 2023 doi:10.20944/preprints202302.0254.v1

Two Area Power System Load Data:

Parameter	Unit	Value
Base MVA	MVA	2000
Pr1, Pr2	MW	2000
P_{L1}, P_{L2}	MW	200
H1,H2	S	5
D1,D2	pu/Hz	0.008
Tg1,Tg2,Tg3,Tg4	S	0.08
Tt1,Tt2, Tt3,Tt4	S	0.3
b1,b2, b3,b4	pu/Hz	0.425
R1,R2, R3,R4	pu/Hz	2.4
T12	pu /Hz	0.55
Pd1	pu	0.01
Kev	Kw/Hz	12
Tev	S	2
Tp	S	24
Kp		120
F	Hz	50

Battery Parameters:

Parameter	Area 1	Area 2
Max. EV Power P_m (Kw)	5	5
$K_{max,}$ (Kw/Hz)	200	200
$SOC_{min,}$ SOC_{max}	30,90	30,90
Delay Time (s) T_{EV}	1	1
No. of EVs	60000	45000